PALEOCEANOGRAPHY, VOL. 17, NO. 1, 1006, 10.1029/2000PA000587, 2002

Response of the thermohaline circulation to cold climates

Zhaomin Wang and Lawrence A. Mysak

Centre for Climate and Global Change Research and Department of Atmospheric and Oceanic Sciences, McGill University, Montreal, Quebec, Canada

Jerry F. McManus

Department of Geology and Geophysics, Woods Hole Oceanographic Institution, Woods Hole, Massachusetts, USA

Received 8 September 2000; revised 20 March 2001; accepted 17 September 2001; published 15 February 2002

[1] A coupled atmosphere-ocean-sea ice-land surface-ice sheet model of intermediate complexity, the so-called McGill Paleoclimate Model, is employed to study the response of the thermohaline circulation (THC) to various global climate coolings, which are realized by increasing the present-day planetary emissivity to various values. Generally, it is found that the response of the THC to global cooling is nonlinear: For a slightly cold climate the THC in the North Atlantic and the Pacific upwelling become intensified. For a very cold climate the THC in the North Atlantic may be weakened or even collapsed. The associated Pacific upwelling for a very cold climate also becomes weak when the THC is weakened, and intermediate deep water may form in the Pacific when the THC is collapsed. Some support for this nonlinear response is found in recent paleoceanographic data. The reduced atmospheric poleward moisture transport due to the global cooling is mainly responsible for the intensification of the THC in the North Atlantic for a slightly cold climate. For a very cold climate the global cooling may lead to a decrease of the meridional surface density gradient and an increase of the vertical density difference (lower layer density minus upper layer density) in the deep water formation region, which can weaken or shut down the THC. It is the temperature-dependent part of the density differences that is mainly responsible for the weakening or shutting down of the THC. The potential influence of surface temperature changes must be taken into account for a full understanding of the role of the THC in the climate system. *INDEX TERMS:* 4267 Oceanography: General: Paleoceanography; *KEYWORDS:* Thermohaline circulation; cold climates; EMIC; ODP Site 980; MPM; nonlinear response

1. Introduction

[2] The global ocean thermohaline circulation (THC) plays an important role in the climate system because of its ability to transport heat poleward. For this reason, variations in the THC transport and structure are of great interest for climate change studies. During the past decade the effects of global warming on the THC have been investigated using coupled global circulation models (GCMs), Earth system models of intermediate complexity (EMICs), and simple (box) climate models [e.g., see *Manabe et al.*, 1991; *Manabe and Stouffer*, 1994; *Stocker and Schmittner*, 1997; *Rahmstorf and Ganopolski*, 1999; *Wang and Mysak*, 2000; *Houghton et al.*, 1997]. The effects of global cooling on the THC have also been studied based on proxy data and climate models. *Sarnthein et al.* [1994] reconstructed the ocean circulation and ocean surface conditions during the Last Glacial Maximum (LGM). *Seidov et al.* [1996] simulated the ocean circulation during the LGM in an ocean only model using reconstructed ocean surface conditions. *Manabe et al.* [1991] integrated a coupled GCM for 100 years with the atmospheric CO_2 concentration reduced by 1%/yr (compounded) and found that this resulted in an intensified THC. *Ganopolski et al.* [1998] simulated the THC during the LGM using the CLIMBER-2 model with the appropriate LGM conditions for ice sheets and atmospheric CO_2 concentration prescribed. *Weaver et al.* [1998] coupled an energy-moisture balance model (EMBM) to an ocean GCM and also simulated the THC during the LGM with prescribed forcing conditions. However, the response of the THC to a wide range of cold climates has never been investigated with a global climate model. The main purpose of this paper is to fill this gap in the literature using a new paleoclimate model of intermediate complexity [*Wang and Mysak*, 2001; *Mysak and Wang*, 2000].

[3] As a first step in this direction, *Winton* [1997] coupled a zonally averaged, one-basin ocean model to an energy balance model (EBM) to study the response of the THC to various cold climates. As the climate gets colder, Winton found that the THC weakens monotonically. He argued that a cold climate may lead to the cooling of the deep ocean and hence a denser deep water. Such denser deep water may prohibit deep convection, which drives the THC. However, because *Winton* [1997] employed an idealized one-basin ocean model, the global conveyor belt cannot be simulated in his model. Also, an active atmospheric hydrological cycle and the growth and decay of continental ice sheets are neglected. Moreover, the role of sea ice in the energy and water budget in the climate system is neglected.

[4] A second purpose of this paper is to consider paleoceanographic evidence for THC modes associated with a range of climatic conditions, particularly those of extreme cold climates. During the last 0.5 million years, orbital forcing and internal mechanisms have combined to produce a range of climatic regimes. This range includes not only intermediate states between the modern Holocene interglaciation and the LGM but also climate states that may have exceeded the severity of the LGM. The global glaciation of marine isotope stage 12 (MIS 12), ~420–440 kyr ago, provides a good example of such an extreme climate for comparison with the model results.

[5] In this paper, we employ a new five-component paleoclimate model [*Wang and Mysak*, 2001] (hereinafter referred to as WM) to study the response of the THC to a range of cold climates. The model consists of an EMBM of the atmosphere coupled to a three-

0883-8305/02/2000PA000587

basin zonally averaged ocean model, a sea ice model, a land surface model, and a dynamic ice sheet model. This model is termed the McGill Paleoclimate Model (MPM) (for further details, see WM and *Mysak and Wang* [2000] (hereinafter referred to as MW)). In addition to the general reasons given above for this study, we are particularly interested in carrying out the following: (1) simulating, for the first time, the THC modes corresponding to the range of cold climates that occurred from the time of initiation of the last glacial (115 ka) to the time of the LGM (21 ka) and those modes also corresponding to extreme cold climates of other peak glacial periods; (2) testing the robustness of the MPM by subjecting it to a large set of sensitivity experiments; (3) comparing the MPM model results with those of other cold climate model simulations; and (4) comparing the simulated cold climate THC modes with those inferred from paleoceanographic data collected from ocean sediment cores.

[6] The remainder of this paper is structured as follows. In section 2 the MPM used is briefly described. In section 3 the THC modes under various cold climate forcings are presented along with their paleoclimate evidence. In section 4 the mechanisms that explain the different THC modes are analyzed. Conclusions are given in section 5.

2. Brief Description of the McGill Paleoclimate Model (MPM) and Integration Scheme

[7] In the work by *Wang and Mysak* [2000] a four-component (atmosphere, ocean, sea ice, and land surface) climate model is developed, which incorporates a variable solar forcing and a seasonal cycle. Three ocean basins, the Antarctic Circumpolar Current region, and the major continents are resolved. However, there is neither an Arctic Ocean nor an Antarctic continent in the model [see *Wang and Mysak*, 2000, Figure 1]. In WM a dynamic ice sheet model with bedrock depression is coupled to the above four-component climate model to produce the five-component MPM. In the MPM, in each 5° latitude band, the model variables are sectorially averaged across the different ocean basins and continents. Below, these five components are briefly described.

2.1. Atmosphere Component

[8] The atmosphere is represented by an EMBM, which is a significant modification of the model of *Fanning and Weaver* [1996]. The present-day monthly mean solar radiation is prescribed at the top of the atmosphere. The monthly mean planetary emissivities are objectively determined from the observed present-day outgoing longwave radiation and the surface air temperature (SAT). The meridional energy and moisture transports are parameterized by a combination of advection and diffusion processes. The zonal heat transport between land and ocean obeys a diffusion law, while the zonal moisture transport is parameterized so that the ocean always supplies moisture to the land. The heat exchanges between the atmosphere and the underlying surface are in the form of longwave radiation and sensible and latent heat. The atmosphere obtains moisture from the underlying surface through evaporation or sublimation. If the relative humidity exceeds a critical value, the excess water vapor will condense and precipitate out, bringing the humidity down to the critical value and releasing latent heat to the atmosphere.

2.2. Ocean Component

[9] In the ocean model, whose domain extends from 75°S to 75°N in the Atlantic sector, zonally averaged advection-diffusion equations for temperature and salinity are employed to predict their time evolution. The velocity components are diagnosed from zonally averaged momentum equations and the continuity equation [*Wright and Stocker*, 1991]. The equation of state is nonlinear [*Wright*, 1997], and the convective adjustment scheme is taken from *Schmidt and Mysak* [1996]. The meridional overturning stream function is diagnosed from the velocity components. Monthly mean wind stress from *Hellerman and Rosenstein* [1983] is applied to the top layer of the model. The zonally averaged east-west pressure gradient is parameterized in terms of the meridional pressure gradient [*Wright and Stocker*, 1991].

2.3. Sea Ice Component

[10] We employ a zero-layer thermodynamic sea ice model without snow in which the sea ice surface temperature and mean thickness are calculated according to *Semtner* [1976], and the ice concentration is predicted using the method of *Hibler* [1979]. The processes of sea ice advection and diffusion are also included; the prescribed meridional advection velocity of sea ice is taken from *Harvey* [1988].

2.4. Land Surface Component

[11] The snow-free land surface temperature is predicted using an energy budget equation under the assumption that the heat capacity of the snow-free land is equivalent to a water depth of 2 m [*Ledley*, 1991]. The snow-covered land surface temperature is predicted using an energy balance equation which neglects the heat capacity of the snow. The snow may accumulate if there is snowfall and the land surface temperature falls to the freezing point. The snow depth is predicted by considering the snow fall, snowmelt, and the sublimation of the snow. The soil moisture and runoff are predicted using the well-known bucket model [*Manabe*, 1969].

2.5. Ice Sheet Component

[12] A vertically integrated mass conservation equation is employed to predict the ice sheet thickness, from which the meridional ice sheet velocity is diagnosed. This equation was first developed by *Oerlemans* [1981] and then further refined by *Gallée et al.* [1992], who introduced a particular form for the lateral discharge in the east-west direction. The bedrock depression is predicted from the approximate isostatic adjustment theory used by *Peltier and Marshall* [1995]. The net accumulation rate is derived from calculating the snow accumulation in the land surface model which, however, takes into consideration the ice sheet elevation-SAT feedback.

2.6. Numerical Integration Scheme

[13] The EMBM, land surface model, and sea ice model are first spun up together under the forcing of monthly mean solar radiation at the top of the atmosphere [*Berger*, 1978] and the zonally averaged monthly mean sea surface temperature (SST) [*Levitus*, 1982]. These models are integrated for 30 years to reach an equilibrium. The ocean model is spun up by restoring the mixed layer temperature and salinity to their observed zonally averaged surface monthly mean values [*Levitus*, 1982] and by applying the zonally averaged *Hellerman and Rosenstein* [1983] monthly mean surface wind stress. The ocean model is integrated for 5000 years to reach an equilibrium. The time step for the EMBM, land surface, and sea ice model is 6 hours, while for the ocean model it is 15 days.

[14] After the equilibrium states are obtained, the ocean model is coupled to the combined EMBM, land surface, and sea ice model using flux adjustments [*Manabe and Stouffer*, 1988, 1994; *Gordon and O'Farrell*, 1997]. Since the equilibrium model ocean temperature in the mixed layer is different from the observed SST under the restoring boundary conditions, the difference between them is calculated and employed to adjust the model mixed layer temperature to be equal to the observed SST. This is similar to the procedure used by *Gordon and O'Farrell* [1997]. The application of this adjustment is necessary because the EMBM is forced by the

SST, which is different from the model mixed layer temperature, and at high latitudes the difference is quite large, and therefore an unrealistic sea ice extent would result. Once the year-round snow cover appears due to the cooling in the northern high latitudes, the ice sheet model is coupled to the other four components. The net ice accumulation rate is derived from the land surface component. The time step for the ice sheet model is 10 years.

3. Response of the THC to Various Cold Climates

3.1. Realization of Cold Climates

[15] The Earth's climate state is significantly controlled by variations in the seasonal distribution of solar energy incident upon the top of the atmosphere [e.g., *Milankovitch*, 1930, 1941]. This "Milankovitch" forcing mechanism is widely believed to be the most important factor responsible for the timing of Quaternary ice ages [e.g., *Hays et al.*, 1976; *Imbrie et al.*, 1984]. However, Milankovitch forcing is relatively weak on the global scale, and hence the adequate simulation of cold climates cannot be realized without the incorporation of many internal feedbacks in the climate system, which involve ice, albedo, water vapor, atmospheric CO_2 concentration, clouds, winds, and vegetation among other elements. Because these feedbacks are not all incorporated into the MPM, cold climates are realized in the model by simply increasing the present-day planetary emissivity [*Wang and Mysak*, 2000] globally and uniformly. This emissivity is increased gradually and linearly over a 5000-year interval until it reaches a prescribed value, which is maintained for another 15 kyr of model integration. Results are presented as the means of the last 5 kyr of the 20-kyr model run. In a future extension of the MPM, feedbacks such as the water vapor-temperature feedback, CO_2-temperature feedback, and cloud-climate feedback will be included, so that the model may be run under the Milankovitch forcing alone.

3.2. Model Results

[16] The planetary emissivity is increased in the above manner by 1%, 2%, 3%,. . ., 10% for 10 sensitivity experiments, respectively. (Note that the radiative forcing for a large increase of the planetary emissivity is quite large if it is calculated using equation (C2) of *Wang and Mysak* [2000]. However, since some internal feedbacks, such as water vapor-temperature feedback and cloud-climate feedback, are excluded, a large radiative forcing may compensate the roles these feedbacks would play.) Hence various cold climates are realized. Table 1 lists the global mean SATs at the end of the model run (the last 5-kyr mean) corresponding to various increases of the planetary emissivity. (For the control run, which simulates present-day conditions, the global mean SAT is 16.27°C, and the maximum THC intensity is 18.9 Sv.) Figure 1 shows the maximum THC intensity in the North Atlantic (the last 5-kyr mean) versus global mean SAT (the last 5-kyr mean) for these 10 experiments. As the climate is first cooled down, the THC becomes intensified. However, after the global mean SAT drops to 12.58°C and the maximum stream function of the THC reaches 25 Sv, the intensity of the THC starts to decrease. For a very large drop (over 8°C) of the global mean SAT (probably not realized during a glacial period) the THC finally collapses. From Figure 1, we may conclude that a slightly cold climate leads to an intensified THC, while a very cold climate may lead to a not strong or even collapsed THC. The latter result only is similar to that found by *Winton* [1997].

Table 1. Global Mean SATs (Last 5-kyr Means) Corresponding to Various Increases of the Planetary Emissivity[a]

Planetary Emissivity Increase, %	Global Mean SAT, °C
1	13.70
2	12.58
3	11.52
4	10.55
5	9.65
6	8.71
7	7.90
8	7.27
9	6.54
10	5.83

[a] For the control run the global mean SAT is 16.27°C.

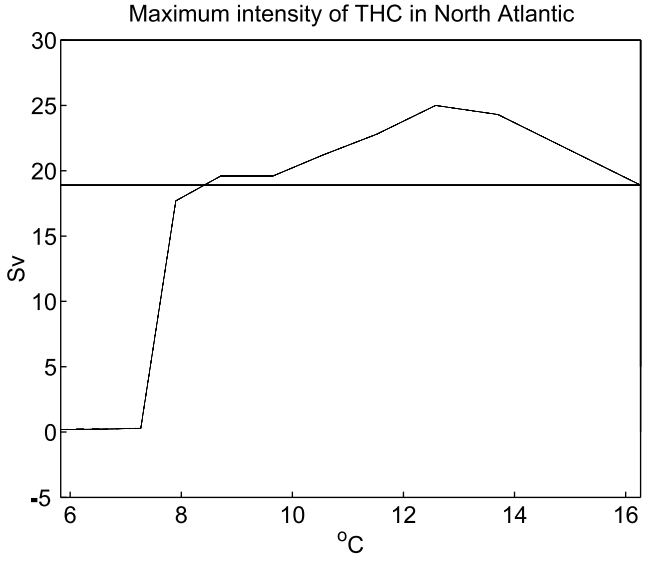

Figure 1. The maximum thermohaline circulation (THC) intensity in the North Atlantic (last 5-kyr mean) versus the global mean surface air temperature (SAT) (last 5-kyr mean).

[17] Figure 2 shows the meridional stream function patterns (last 5-kyr means) in the Atlantic and the Pacific Oceans for the control run (global mean SAT of 16.27°C) (Figures 2a and 2b), a 2% planetary emissivity increase (global mean SAT of 12.58°C) (Figures 2c and 2d), a 5% increase (global mean SAT of 9.65°C) (Figures 2e and 2f), and an 8% increase (global mean SAT of 7.27°C) (Figures 2g and 2h). For the slightly cold climate (Figures 2c and 2d) the THC in the North Atlantic is intensified, and the northward penetration of the Antarctic Bottom Water (AABW) is slightly reduced. The upwelling in the Pacific Ocean is also intensified in this case, which is consistent with a strong conveyor belt. For a colder climate (Figures 2e and 2f) the maximum stream function value is very close to that of the control run and the depth of the North Atlantic Deep Water (NADW) formation is almost the same as in the control run. For the extremely cold climate (global mean SAT dropping to 7.27°C) the THC is collapsed, and intermediate deep water formation (down to 2000 m) occurs in the Northern Pacific. The latter may be due to the very cold Northern Pacific water. *Marotzke and Willebrand* [1991] also found deep water formation in the North Pacific when the North Atlantic THC collapses by perturbing the freshwater forcing.

[18] Note that for two of the cold climate runs (Figures 2c and 2d and 2e and 2f) the NADW formation region shifts southward to 62.5°N, which is mainly due to the insulation effect of the sea ice cover on the air-sea heat exchange. In the LGM simulation of *Ganopolski et al.* [1998] the NADW formation region shifts southward to 45°N, while in that of *Weaver et al.* [1998], the NADW formation region during the LGM remains the same as that during the present day. However, if we increase the sea ice advection velocity (this velocity is prescribed as the present-day value [see *Wang and Mysak*, 2000]) by four times, the NADW

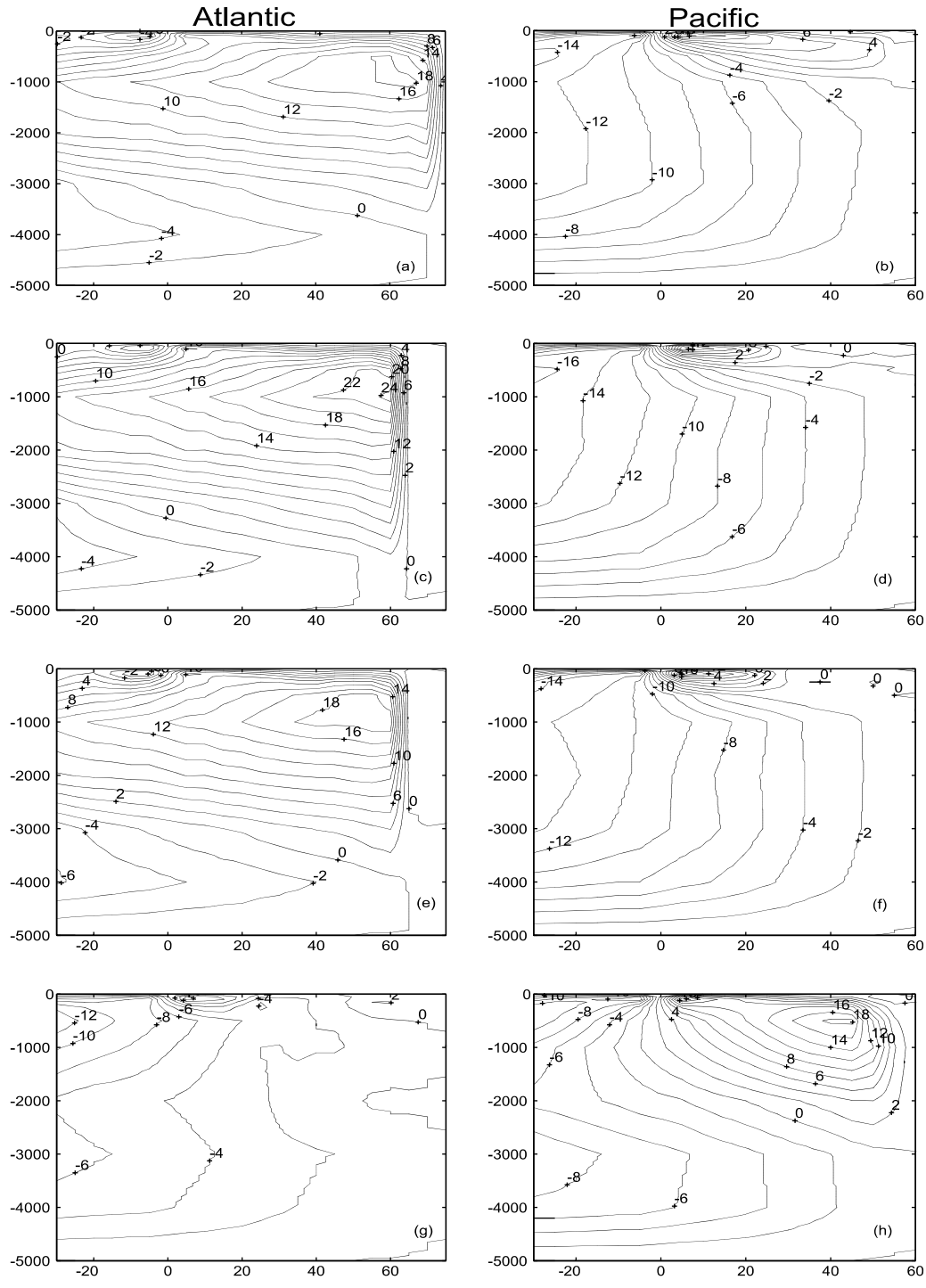

Figure 2. The annual mean stream function patterns (last 5-kyr means) for the Atlantic Ocean (Figures 2a, 2c, 2e, and 2g) and Pacific Ocean (Figures 2b, 2d, 2f, and 2h) corresponding to four global mean SATs: (a and b) 16.27°C, (c and d) 12.58°C, (e and f) 9.65°C, and (g and h) 7.27°C. The contour interval is 2 Sv.

formation region shifts back to the original location as shown in Figure 2a (not shown). For the 5% planetary emissivity increase run (Figures 2e and 2f) the sea ice in the North Atlantic Ocean may advance to 57.5°N in winter. The increase of the sea ice advection velocity leads to an enhanced southward freshwater transport. This increases the surface salinity in the very northern high latitudes and decreases the surface salinity in the relatively southern region or sea ice margin. (This brine rejection effect was studied by *Lohmann and Gerdes* [1998] and was thought to be minor; however, another study [*van Kreveld et al.*, 2000] showed the importance of this effect.) This means that deep water may form under the sea ice for quite a large southward sea ice transport in the MPM. However, without the incorporation of the sea ice advection process, *Weaver et al.* [1998] also simulated deep water formation under the sea ice. Recent reconstruction data [*Dokken and Jansen*, 1999] show that during cold phases (stadials) of the latter part of the last glacial

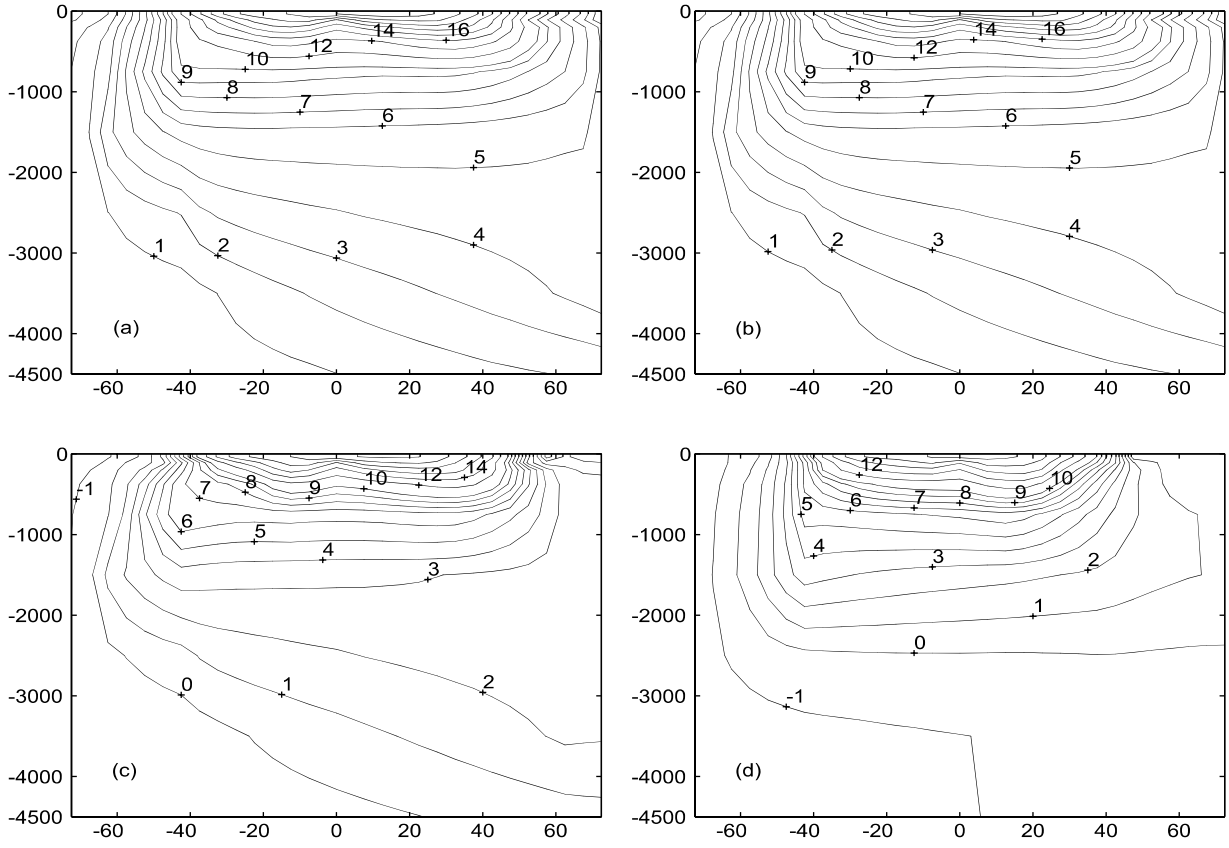

Figure 3. The annual mean temperature field for the Atlantic Ocean corresponding to four global mean SATs: (a) 16.27°C, (b) 12.58°C, (c) 9.65°C, and (d) 7.27°C. The contour interval is 1°C below 10°C or 2°C above 10°C.

period (60–10 kyr ago), the North Atlantic Deep Water (NADW) might be driven by salt rejection when sea ice formed. A more accurate simulation of the NADW formation location needs a better resolution of air-ocean-sea ice interactions.

[19] It is also worth pointing out that in the work of *Weaver et al.* [1998] a 3.2°C drop of the global mean SAT leads to the weakening of the THC in the North Atlantic by 6 Sv, while in the work of *Ganopolski et al.* [1998] the 6.2°C drop of the global mean SAT does not change the maximum intensity of the THC in the North Atlantic. In the MPM results (Figure 2e) the 6.62°C drop of the global mean SAT also leads to no change of the maximum intensity of the THC in the North Atlantic.

[20] Corresponding North Atlantic Ocean temperature and salinity fields (last 5-kyr means) are shown in Figures 3 and 4, respectively, for the control run and for 2, 5, and 8% increases of the planetary emissivity. (The present-day (control run) temperature and salinity fields in the other oceans are given by *Stocker et al.* [1992].) As the global mean SAT drops, in the southern high latitudes, the 0°C contour shifts northward; in the northern high latitudes the 5°C contour shifts southward. Both indicate the equatorward expansion of sea ice. Another important feature is that the deep ocean temperature drops as the SAT drops. In Figure 3d, owing to the collapse of the THC the cold Antarctic Bottom Water (AABW) penetrates extremely northward, and the deep ocean becomes very cold. Figure 4 shows that the ocean salinity generally becomes larger as the SAT drops mainly due to the growth of continental ice and formation of sea ice. In Figure 4d the northern high latitudes become very fresh owing to the significantly reduced northward salt transport for a collapsed THC.

[21] Figure 5 shows the latitudinal distributions of the SAT for the control run and for 2, 5, and 8% increases of the planetary emissivity. As the emissivity increases, the SAT drop is quite uniform with latitude, except in the northern high latitudes for the control run as compared to the 2% increase run. In this region the SAT drop from the control run to the 2% increase run is relatively large, mainly because of a significant southward advance of sea ice in the North Atlantic Ocean and the growth of ice sheets. In the Southern Hemisphere, for the 5 and 8% increase runs, the SAT drop is much smaller than that in the Northern Hemisphere because of the collapse of the THC. This is mainly due to the significant heat transport to the Southern Hemisphere for a collapsed THC [see *Stocker*, 2000; *Wang and Mysak*, 2000, Figure 18].

[22] Figure 6 shows the latitudinal distribution of the atmospheric meridional transports of the sensible heat (Figure 6a) and moisture (Figure 6b) for the four global mean SAT values used in Figure 5. The changes of the sensible heat transport in the lower latitudes are small, mainly because the meridional wind is prescribed in that region (as well as everywhere else). However, the increases of the sensible heat transport in the middle and high latitudes are relatively large because of the increased meridional temperature gradients. In contrast, both the equatorward moisture transport in the lower latitudes and the poleward moisture transport in the middle latitudes are reduced as the climate is cooled down. The reduction of the equatorward moisture transport is mainly due to the drop of the moisture content for cold climates, while the reduction of the poleward moisture transport is largely due to the decrease of the meridional surface specific humidity gradient [*Wang and Mysak*, 2000].

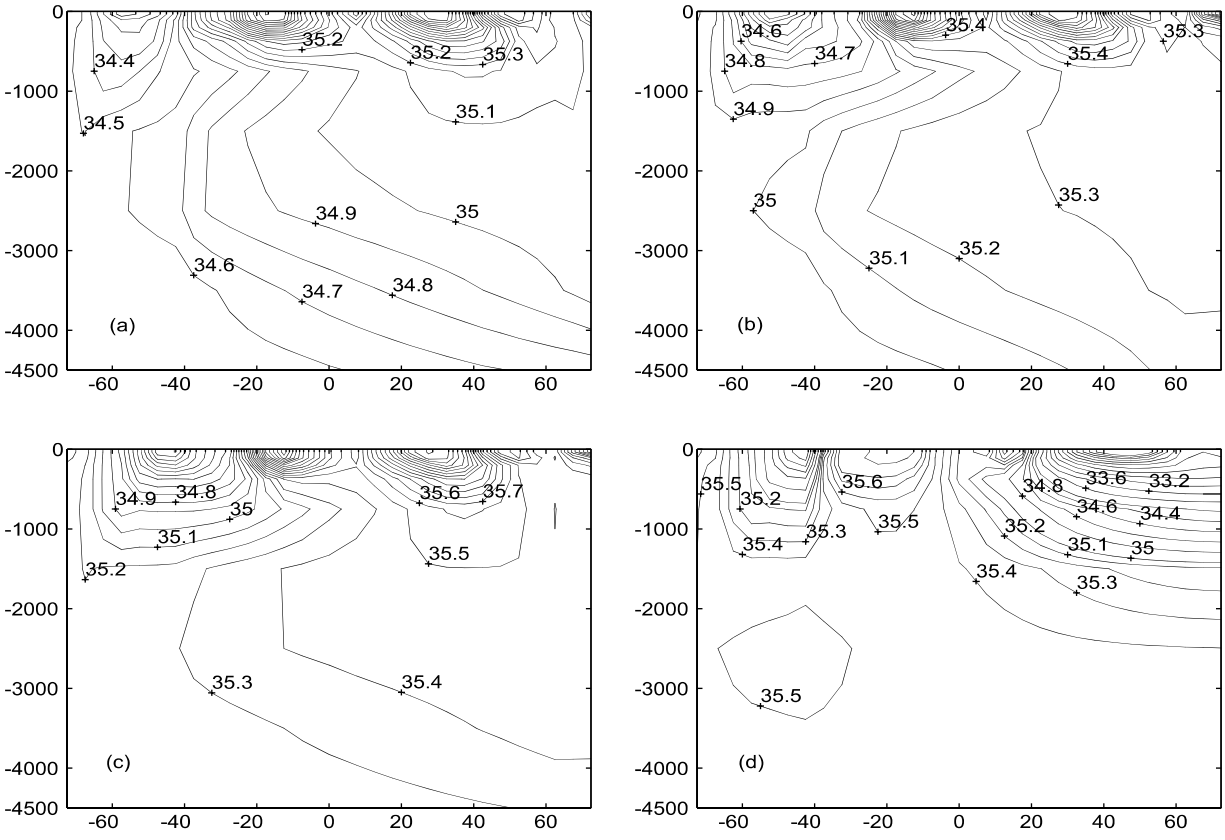

Figure 4. The annual mean salinity fields for the Atlantic Ocean corresponding to four global mean SATs: (a) 16.27°C, (b) 12.58°C, (c) 9.65°C, and (d) 7.27°C. The contour interval is 0.1 psu for Figures 4a–4c, while for Figure 4d it is 0.1 psu if salinity is >35 psu, 0.2 psu if salinity is <35 psu and >34 psu, and 0.4 psu if salinity is <34 psu.

3.3. Evidence for Cold Climate THC Modes From Paleoclimate Data

[23] The response of the THC to various cold climates in the MPM suggests that the inception phase or early stage of a glacial period is likely to be associated with a strong THC and that during a peak glacial period the THC would not be stronger than the present-day THC. The model results also imply that once the climate is very cold, additional cooling would only further weaken the THC and even lead to a collapsed state.

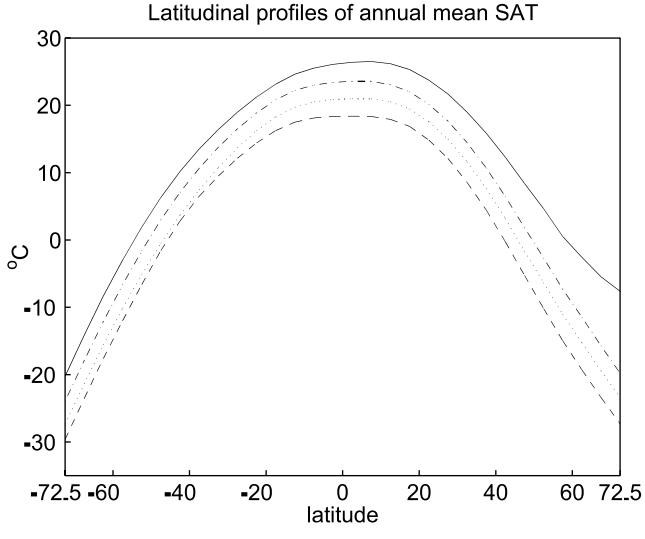

Figure 5. The latitudinal profiles of the SAT corresponding to four global mean values of 16.27°C (solid line), 12.58°C (dot-dashed line), 9.65°C (dotted line), and 7.27°C (dashed line). These correspond to the control run and to 2, 5, and 8% increases of the planetary emissivity, respectively.

[24] A number of paleoclimatic reconstructions of the glacial North Atlantic have demonstrated that during the cold conditions of the LGM, intermediate waters were ventilated from the north, while deep waters had a stronger southern source influence [*Boyle and Keigwin*, 1987; *Oppo and Fairbanks*, 1987; *Duplessy et al.*, 1988; *Oppo and Lehman*, 1993; *Sarnthein et al.*, 1994]. Although it can be argued that such a vertically partitioned configuration might be associated with a similarly vigorous THC as during warm times [e.g., *Yu et al.*, 1996], other lines of evidence indicate that a weakened THC characterized the cold LGM [e.g., *Shackleton et al.*, 1988; *Lynch-Steiglitz et al.*, 1999].

[25] For comparison of the model results with a range of paleoclimate data we have chosen the 0.5 million year record from ODP Site 980 [Oppo et al. , 1998; McManus et al., 1999], which extends beyond the LGM into previous glaciations of varying severity. Foraminiferal stable isotopes at this high-sedimentation site in the North Atlantic provide, at one location, detailed evidence for global glaciation, regional SST, and deep water mass influences associated with the THC (Figure 7). Although no single record can document global atmospheric mean temperatures, Site 980 SST compares favorably with records from other regions [*McManus et al.*, 1998, 1999].

[26] The 0.5 million year interval includes five large glacial cycles of ~100 kyr, paced by orbital eccentricity. Benthic $\delta^{18}O$ clearly delineates the glacial (even) and interglacial (odd) marine

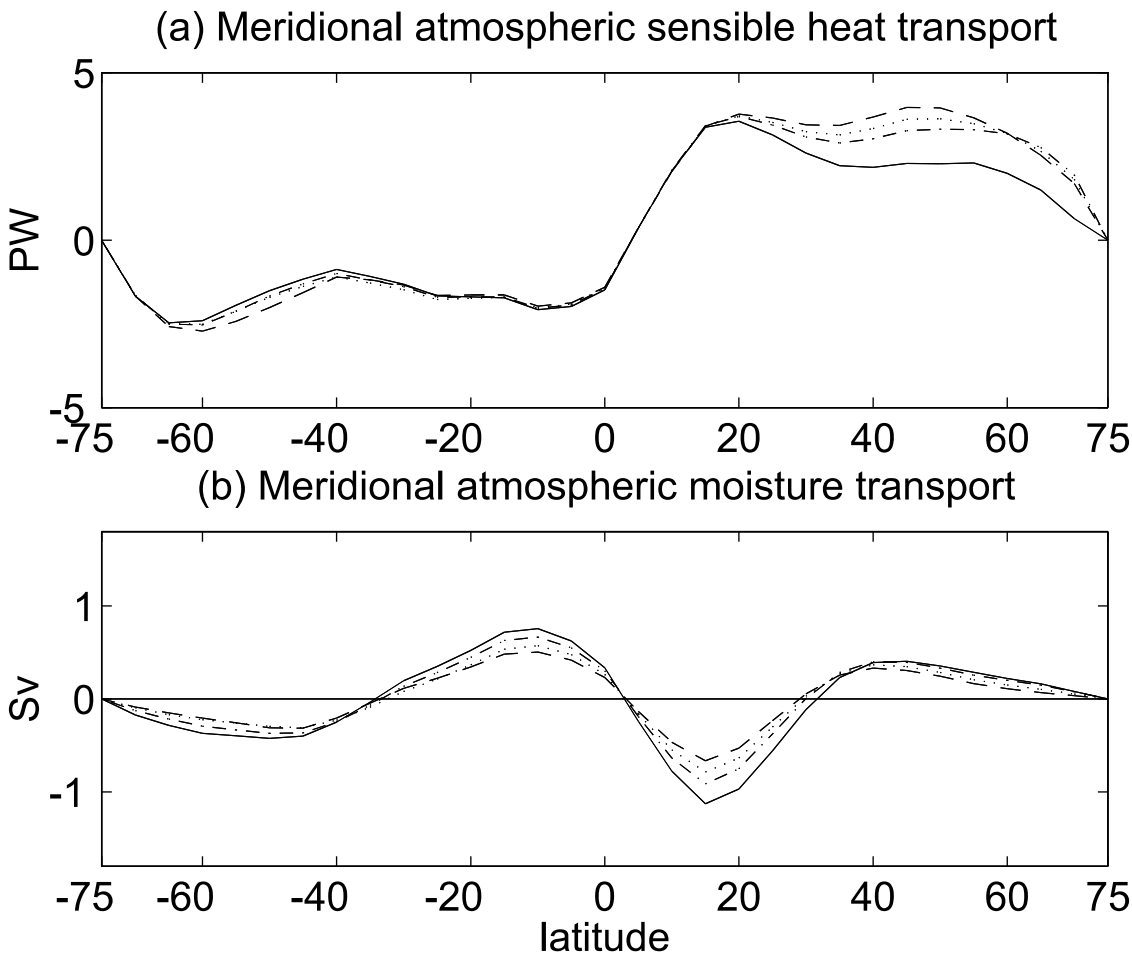

Figure 6. The meridional atmospheric (a) sensible heat transports and (b) moisture transports corresponding to four global mean SAT values of 16.27°C (solid line), 12.58°C (dot-dashed line), 9.65°C (dotted line), and 7.27°C (dashed line).

isotope stages (MIS). At Site 980, as in previous comparisons [e.g., *Shackleton*, 1987; *Raymo*, 1997], MIS 1, 5e, 9, and 11 are the most extreme interglacial intervals, and MIS 2, 6, 10, and 12 are the most glacial, with MIS 12 being the most extreme.

[27] Estimates of SST were previously derived from foraminiferal $\delta^{18}O$, adjusted by a varying portion of benthic $\delta^{18}O$ to account for ice volume and deep ocean temperature [*McManus et al.*, 1999]. The SST values display significant oscillations (3°–6°C) on short timescales and even larger glacial-interglacial (G-IG) contrasts. At this site the LGM was 8°C colder than the subsequent warm Holocene interglacial. MIS 4, 6, 8, and 10 also experienced SST depressions of 6°–8°C. The coldest SST occurred during MIS 12 and represented ~10°C of cooling. Warm SST, reaching 14°–15°C, characterized each peak interglacial interval. Slightly cooler temperatures (11°–13°C) occurred throughout the record, particularly during intervals of nonpeak interglaciations, such as much of MIS 5a-d, late MIS 7, late MIS 9, and MIS 13.

[28] Benthic foraminiferal $\delta^{13}C$ from Site 980 is applied as a proxy for the strength of the THC [*Oppo et al.*, 1998; *McManus et al.*, 1999] while acknowledging that it is also sensitive to the potentially competing influences of long-term modulation of the carbon cycle [e.g., *Sarnthein and Tiedemann*, 1989], redistribution of organic carbon among global reservoirs [*Shackleton*, 1977], air-sea exchange fractionation [*Broecker and Peng*, 1982; *Lynch-Steiglitz and Fairbanks*, 1994], preformed nutrient content of the ventilating waters [e.g., *Oppo and Fairbanks*, 1987; *Charles and Fairbanks*, 1992], episodic productivity [*Mackensen et al.*, 1993] and carbonate ion concentration [*Spero et al.*, 1997]. For these reasons, the $\delta^{13}C$ at Site 980 must be considered merely as a qualitative assessment of the bottom water nutrient signature and one that also integrates other influences in addition to the THC intensity.

[29] Both the SST and the benthic $\delta^{13}C$ oscillate throughout the last 0.5 million years, consistent with a persistent climate-ocean variability on millennial timescales [*McManus et al.*, 1999]. The glacial intervals display the most SST variability and also the coldest temperatures. They are also generally associated with the lowest $\delta^{13}C$ and therefore a weaker THC. Because the glacial $\delta^{13}C$ values typically contrast with interglacial values by 0.5–1‰, they exceed the inferred 0.3‰ change due to carbon redistribution [*Shackleton*, 1977; *Duplessy et al.*, 1988] and must also have an important component of a weakened THC. This association of diminished THC with the cold SST of glaciation has long been noted [e.g., *Mix and Fairbanks*, 1985; *Boyle and Keigwin*, 1987; *Boyle and Rosener*, 1990]. An important point here is that while the observed SST changes may be interpreted as being driven by THC changes, they are also consistent with the MPM results predicting that limited strength of THC may also be a response to climate conditions, rather than a cause. In reality, there is likely

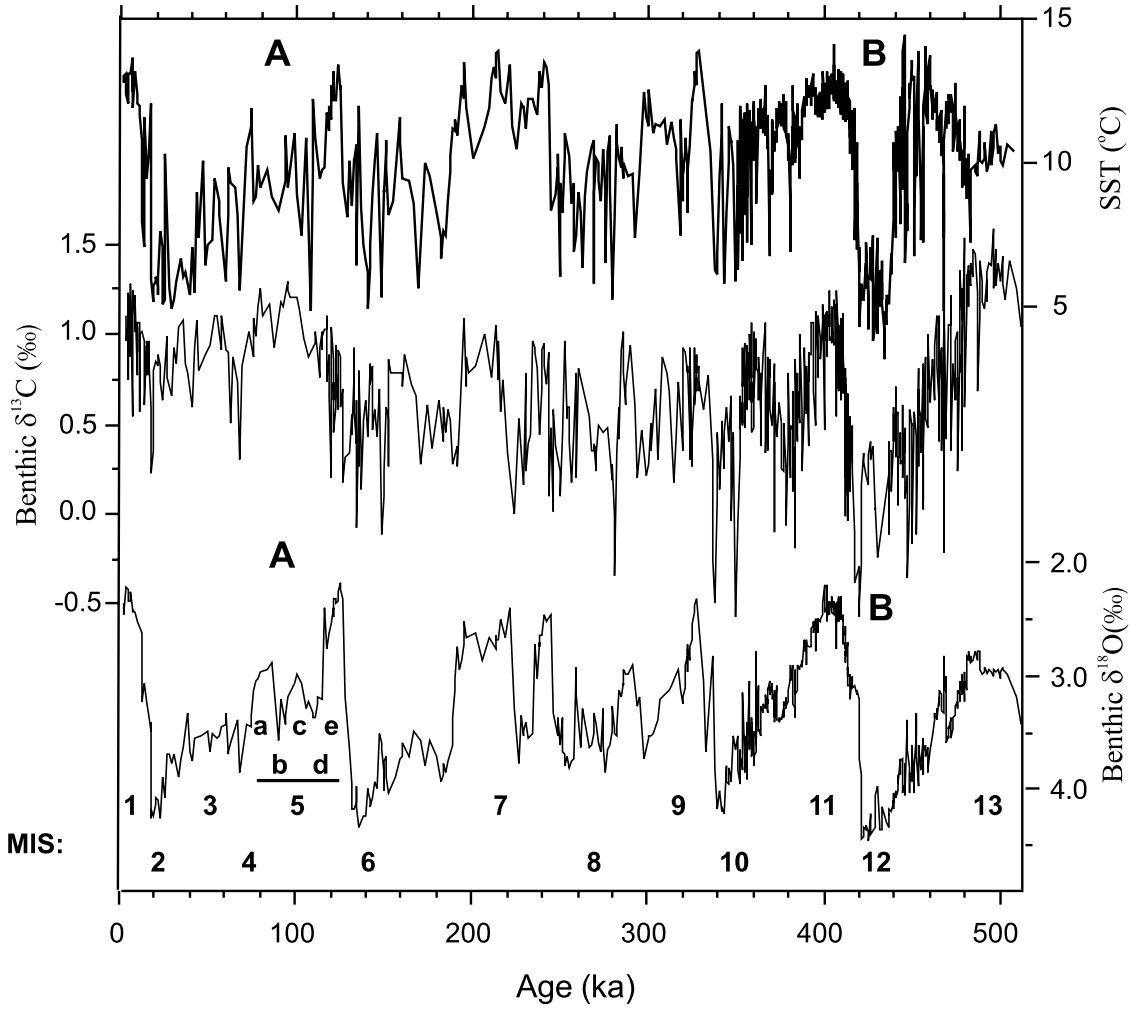

Figure 7. Paleoclimate data from Ocean Drilling Program (ODP) Site 980 (55°29′N, 14°42′W, 2179 m) over the last 0.5 million years [*Oppo et al.*, 1998; *McManus et al.*, 1999]. Benthic data were obtained from *Cibicidoides wuellerstorfi*. SST data were derived from $\delta^{18}O$ measurements of the planktonic foraminifera *Neogloboquadrina pachyderma* dextral, adjusted for ice volume using the benthic $\delta^{18}O$. "A" (MIS 5a–5c, ~80–100 kyr) and "B" (MIS 12, ~420–440 kyr) indicate portions of the record demonstrating that the strongest THC is associated with moderate SST and the weakest THC is associated with coldest SST. Bold numerals indicate marine isotope stages (MIS).

to be a THC-climate feedback that converges on preferred SST-THC modes. The MPM result here demonstrates the climate-driven component.

[30] Prominent increases in $\delta^{13}C$ are associated with the moderate temperatures that occur within the G-IG cycles following the initial peak SST of MIS 7, 9, and 11. During MIS 13, similarly moderate SSTs occur along with the highest $\delta^{13}C$ of the entire record. Within MIS 5 the $\delta^{13}C$ values achieved during the time of warmest SST are followed by a brief, sharp reduction and then a rapid return to even higher values than previously. The strengthened THC during the glacial inception of the MIS 5e/5d transition [*Duplessy and Shackleton*, 1985] has been suggested to play an important twofold role by providing the moisture source required to facilitate rapid ice growth [*Ruddiman et al.*, 1980] and in ameliorating the SST decline brought about by declining insolation and growing ice sheets [*McManus et al.*, 2002]. At Site 980, benthic $\delta^{13}C$ continued to increase to even higher values during the subsequent interstadial substages MIS 5a and 5c (Figure 7, A). This longer-term trend within the broadly defined interglacial MIS 5 has also been recognized elsewhere [*Keigwin and Boyle*, 1985; *Labeyrie et al.*, 1987; *Oppo and Lehman*, 1995; *Oppo et al.*, 1997; *Vidal et al.*, 1997]. *Chapman and Shackleton* [1998] specifically argued that the long gradual isotopic increase might reflect an increasing THC associated with decreasing SST, although alternative explanations exist. These include a mean ocean trend in $\delta^{13}C$, which is consistent with a small shift over this interval in epifaunal benthics from Site 849 in the Pacific [*Mix et al.*, 1995] or a general shift in the $\delta^{13}C$ of surface waters that eventually ventilate the deep ocean. Such a shift in surface $\delta^{13}C$ is widely evident from the tropics [*Curry and Crowley*, 1987] to the sub-Arctic [*Fronval and Jansen*, 1997] and in the Atlantic [*Labeyrie et al.*, 1999], Pacific [*Shackleton et al.*, 1983], Indian [*Shackleton and Pisias*, 1985], and Southern Oceans [*Ninnemann et al.*, 1999].

[31] Perhaps the most striking support for the MPM results comes from the extreme glaciation of MIS 12. SST was reduced by 10°C during this interval, making it not only the most glaciated

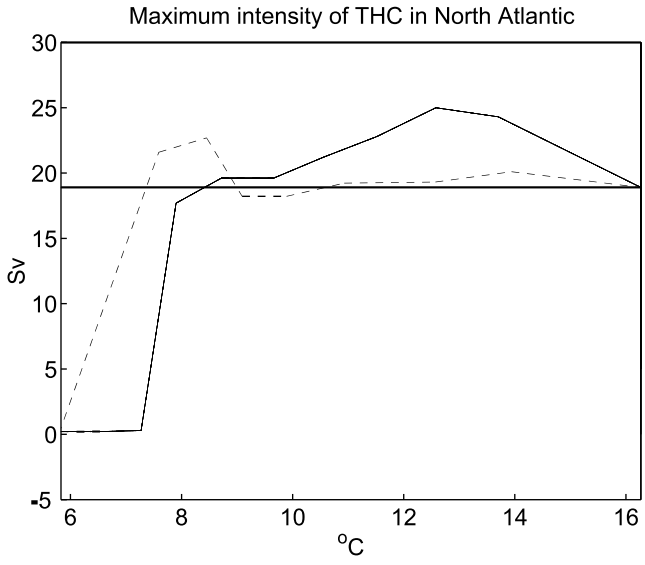

Figure 8. The maximum THC intensity in the North Atlantic versus the global mean SAT for fixed oceanic freshwater flux runs (dashed line). The solid line is taken from Figure 1.

interval of the last 0.5 million years, based on sea level proxies [*Shackleton*, 1987; *Rohling et al.*, 1998] but also the coldest time in the North Atlantic and possibly globally [*McManus et al.*, 1999]. At Site 980 these extremely cold SSTs were accompanied by dramatically diminished $\delta^{13}C$, suggesting a marked drop in THC strength (Figure 7, B). The $\delta^{13}C$ declined to values of $\sim$0.0‰ that are not found anywhere in the modern Atlantic Ocean [*Kroopnick*, 1980]. Brief excursions during the coldest intervals reach values of -0.5‰. Although the severe climate and increased ice volume of MIS 12 would likely have decreased the terrestrial carbon reservoir, leading to a transfer of isotopically light carbon to the oceans, as inferred for the LGM [*Shackleton et al.*, 1983], the amplitude of the $\delta^{13}C$ shift across MIS 12 at Site 980 is, nevertheless, >3 times the size of the global shift during the LGM, when terrestrial productivity was reduced by $\sim$33% of modern (G. Hoffmann et al., Personal communication, 2001).

[32] The dramatic shift in $\delta^{13}C$ during MIS 12 was also evident in the THC index constructed by *Raymo et al.* [1990], who found that deep North Atlantic values most nearly approached Pacific values at that time. A similar result was obtained by *Flower et al.* [2000] using additional cores with improved resolution and epifaunal analyses. The combined SST and $\delta^{13}C$ data of Site 980 allow comparisons throughout the interval containing MIS 12 (Figure 7, B). The moderate SST values of MIS 13 are associated with the highest $\delta^{13}C$. A subsequent increase in SST during late MIS 13 is accompanied by a decline in $\delta^{13}C$, to values of $\sim$1.0‰ that are comparable to modern NADW values. Both SST and $\delta^{13}C$ reach minima during MIS 12 before returning to values that are also similar to modern in MIS 11 (13°C, 1.0‰). Throughout this particular sequence, as during MIS 5–6, the paleoclimate data are consistent with the MPM results that suggest that while the warmest SST is associated with a relatively strong THC, the strongest THC is associated with moderate SST, and extreme cold SST is associated with the weakest THC. Alternative explanations apply, but at this point the MPM results must be considered among the viable interpretations. This comparison underscores the importance of confirming the $\delta^{13}C$ data and the need to resolve existing ambiguities in the sedimentary record of past variations in the strength of THC, particularly during a range of cold climates.

4. Mechanistic Analysis

[33] In this section, we analyze the possible mechanisms which are responsible for the responses of the THC (Figure 1) to cold climates. In particular, we examine the role of the hydrologic cycle in determining the various THC modes and delve into the reasons for the collapse of the THC.

4.1. Role of Hydrologic Cycle

[34] From Figure 6b we note that for colder SAT values the atmospheric poleward moisture transport is reduced in the middle latitudes upon cooling. This is qualitatively consistent with the results from a coupled atmosphere-ocean GCM [*Manabe et al.*, 1991]. This occurs in the MPM because of the reduced gradient of the surface specific humidity in a cold climate [*Wang and Mysak*, 2000]. Also, as the climate is cooled down, the ice sheets begin to grow (see WM, section 3, and Figure 2) and hence the freshwater flux into the ocean is reduced. However, the reduction of this freshwater flux to the ocean due to the ice sheet growth is much smaller than that due to the reduced atmospheric poleward moisture transport, when the ice sheets reach quasi-equilibrium states. (During the first 10 kyr of the last glacial period, which is a rapid ice sheet growth phase, sea level dropped $\sim$50 m [*Johnson and Andrews*, 1979]. The resulting oceanic freshwater flux reduction is $\sim$0.057 Sv. However, in the MPM, the ice sheet growth at the end of the model runs is much smaller than the rapid ice sheet growth during the first 10 kyr of the last glacial period [WM]. In Figure 6b, at 50°N, the difference of the moisture transport between the value of the control run and that of the run with the global mean SAT of 7.27°C is 0.10 Sv.)

[35] The reduced freshwater flux into the ocean will increase the surface salinity in the subpolar North Atlantic Ocean. Hence, the NADW is enhanced and the THC is intensified. This mechanism is responsible for an intensified THC due to global cooling in the coupled atmosphere-ocean GCM of *Manabe et al.* [1991]. In order to test the role of the active atmospheric hydrological cycle in the MPM, we did another set of sensitivity experiments, which are similar to those in Figure 1 except that the freshwater flux into the ocean is fixed as that in the control run. By doing so the effects of the atmospheric hydrological cycle, ice sheet growth, and the freshwater transport related to sea ice are removed.

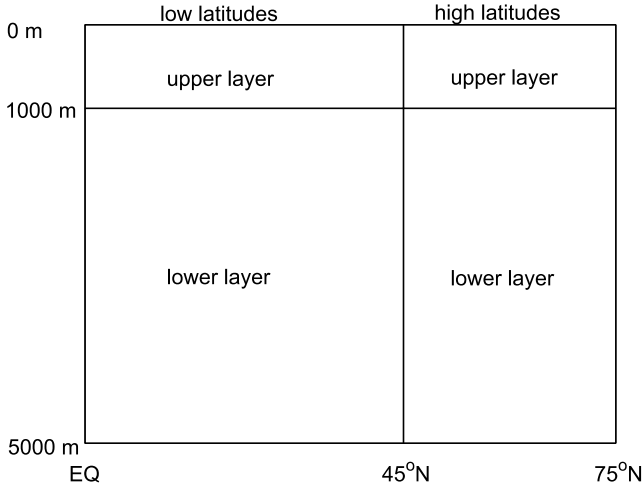

Figure 9. The definition sketch for upper and lower layers and low and high latitudes.

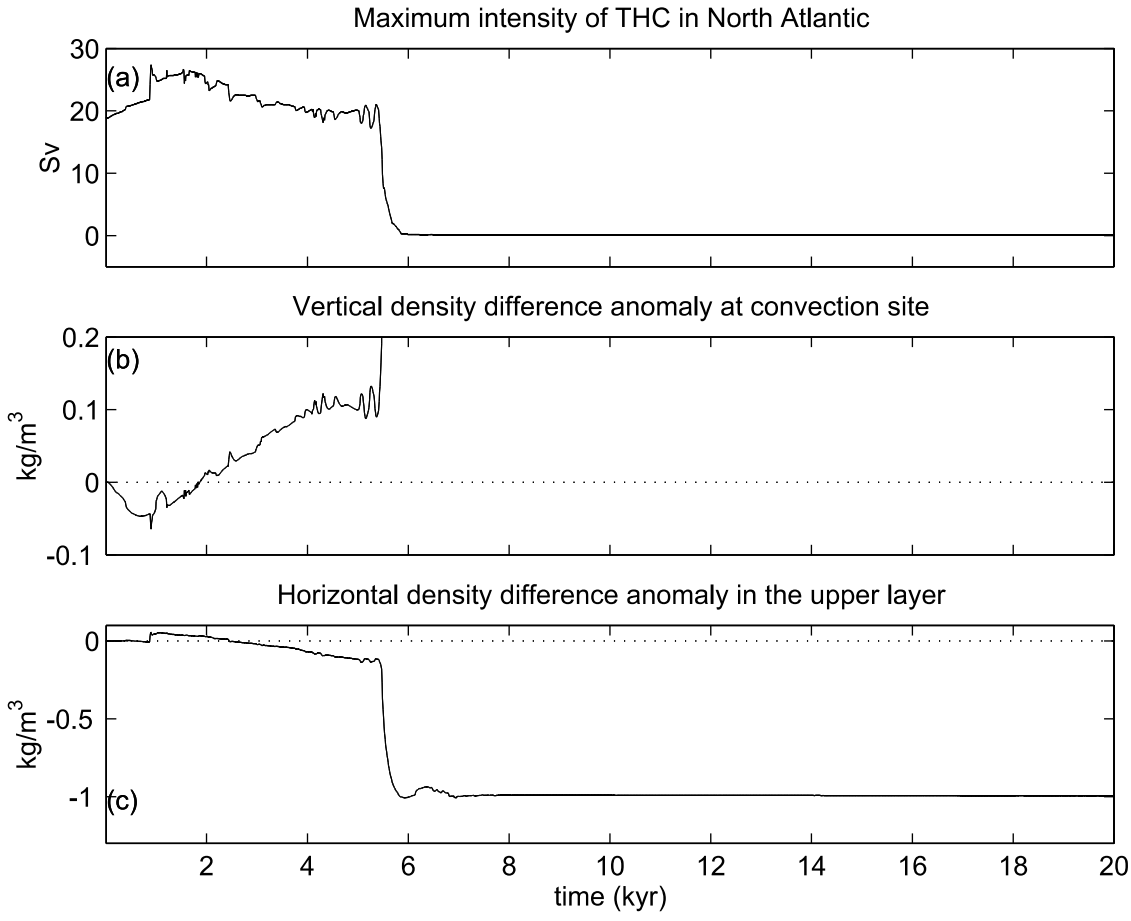

Figure 10. The time series of (a) the maximum THC intensity in the North Atlantic, (b) the vertical density difference (lower layer density minus upper layer density) anomaly relative to the same initial density difference at the convection site (around 62.5°N), and (c) the horizontal density difference (high-latitude density minus low-latitude density) anomaly relative to the same initial density difference in the upper layer for the experiment which has the 8% increase of the planetary emissity and global mean SAT of 7.27°C at the end of the model run. Note that the hydrological cycle is not fixed.

[36] The dashed line in Figure 8 shows the response of the maximum intensity of the THC in the North Atlantic to various cold climates for a fixed freshwater flux. Clearly, this intensity does not change very much as the climate is cooled down to ~9°C, in contrast to the case with an active hydrological cycle (solid line). Although the intensity of the THC jumps up to 22.5 Sv after the global mean SAT drops below 9°C, the THC still collapses for an extremely cold climate. This result strongly suggests that the active hydrological cycle is responsible for the intensification of the THC for a slightly cold climate.

4.2. Why the THC Becomes Weak and Then Collapses

[37] From Figure 1 we observe that for very cold climates (global mean SAT below 7.9°C) the THC becomes weaker than for the control run and collapses when the global mean SAT is 7.27°C or lower. In order to understand this the time series of the maximum THC intensity in the North Atlantic, the difference between the lower and upper layer densities relative to the same initial density difference at the convection site (around 62.5°N), and the difference between the high and low latitude density relative to the same initial density difference (see Figure 9 for definitions of the upper and lower layers, low and high latitudes) are plotted in Figure 10 for the experiment which has the global mean SAT of 7.27°C (last 5-kyr mean). This corresponds to the planetary emissivity increase of 8%. From Figure 10a we note that the intensity of the THC increases first and then begins to decrease at around 2 kyr as the climate cools down, which is consistent with the results derived from Figure 1. Corresponding to the intensity change of the THC, the vertical density difference anomaly becomes negative at first (corresponding to a stronger THC) and then becomes positive at around 2 kyr (Figure 10b). Finally, at around 5.5 kyr the vertical density difference anomaly approaches a critical value beyond which the THC collapses. From Figure 10c we observe the opposite behavior of the horizontal density difference anomaly. The anomaly first becomes positive, then goes negative at around 2.5 kyr, and finally approaches a critical value at around 5.5 kyr.

[38] On the basis of above results we suggest that the change of the THC intensity is driven by density changes, which in turn, are controlled by the climate change. A natural question that arises is, what is the relative importance of the vertical density difference anomaly at the convection site and the horizontal density difference anomaly in the upper layer? In the work by *Winton* [1997], on the basis of his box model and a zonally averaged ocean model study, the vertical stratification determined the NADW formation rate, which is mainly responsible for the change of the THC. However,

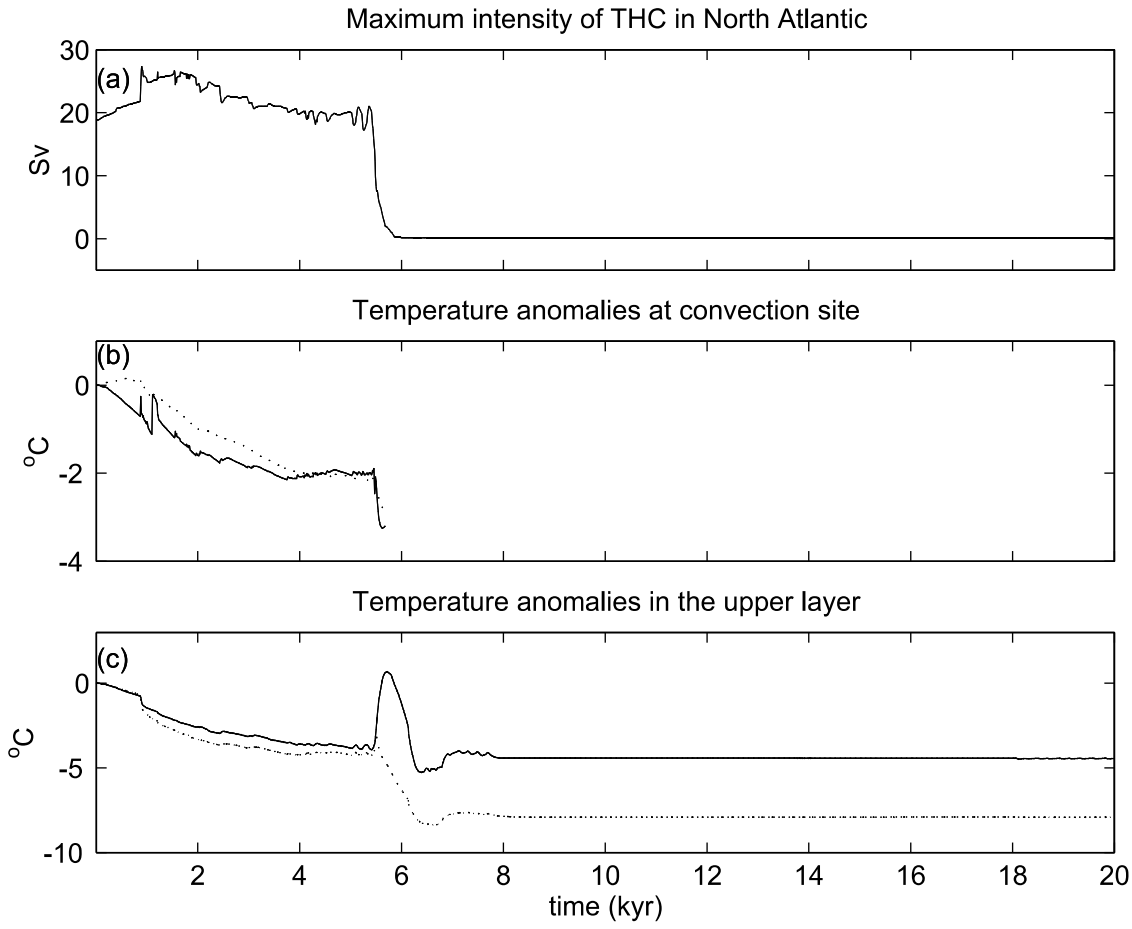

Figure 11. The time series of (a) the maximum THC intensity in the North Atlantic, (b) the upper and lower layer temperature anomalies relative to their initial values at the convection site (around 62.5°N; dotted line corresponds to lower layer; solid line corresponds to upper layer), and (c) the low- and high-latitude temperature anomalies relative to their initial values in the upper layer (dotted line corresponds to high latitudes; solid line corresponds to low latitudes) for the same experiment as in Figure 10.

in the work by *Hughes and Weaver* [1994], a linear relationship is found between the intensity of THC and the meridional gradient of vertically integrated steric height; in the box model studies of *Rahmstorf* [1996], the horizontal density gradient plays a dominant role for the THC intensity change. In the work by *Prange et al.* [1997], although convective processes are not resolved, the THC becomes weak when the global temperature decreases. Here we cannot separate the effects due to the two types of density change. However, they appear to have similar effects on the THC in the MPM.

4.3. Is the THC Collapse Mainly Due to Temperature or Salinity Changes?

[39] In this section, we will argue that temperature changes are mainly responsible for the weakening and ultimate collapse of the THC. First, we observe that the reduced poleward atmospheric moisture transport shown in Figure 6b together with the growth of ice sheets will reduce the freshwater flux into the subpolar North Atlantic Ocean and hence increase the surface salinity there. Also, from Figure 8, for the experiment with fixed freshwater flux, the THC is still collapsed for very cold climates. Therefore the salinity change may not contribute to the weakening and ultimate collapse of the THC. In fact, for the experiment which has the global mean SAT of 7.27°C, the largest salinity increase at 52.5°N (to the south of the NADW formation region) is +0.2 psu (not shown), which is due to both the reduced freshwater flux into the ocean and the intensified THC for a slightly cold climate. (However, at the convection site (62.5°N) the salinity is slightly reduced (by ~0.1 psu) even when the THC is intensified, which is mainly due to the southward freshwater transport associated with sea ice; at 72.5°N the salinity reduction is much larger (up to 0.7 psu), which is mainly due to the southward shift of the NADW formation region. Another set of sensitivity experiments without salt rejection of sea ice shows an increase of salinity at the convection site, a more intensified THC (by several Sv) and also a southward shift of the NADW formation region (not shown). Therefore the southward freshwater transport associated with sea ice has a slight weakening effect on the THC in the MPM results.)

[40] In Figure 11 we now show the time series of the maximum intensity of the THC, the upper and lower layer temperatures relative to their initial values at the convection site, and the low and high latitude upper layer temperatures relative to their initial values. We observe that at the convection site the upper layer temperature anomaly is larger than that of the lower layer until 4 kyr. However, after 4 kyr, the anomalies of the upper and lower layer temperature are quite similar. This is mainly due to the fact that sea ice may insulate the air-sea heat exchange and hence prevent the surface from further cooling, i.e., the surface cooling may be "saturated." Taking into account the role of pressure, the density change in the lower layer is larger than that

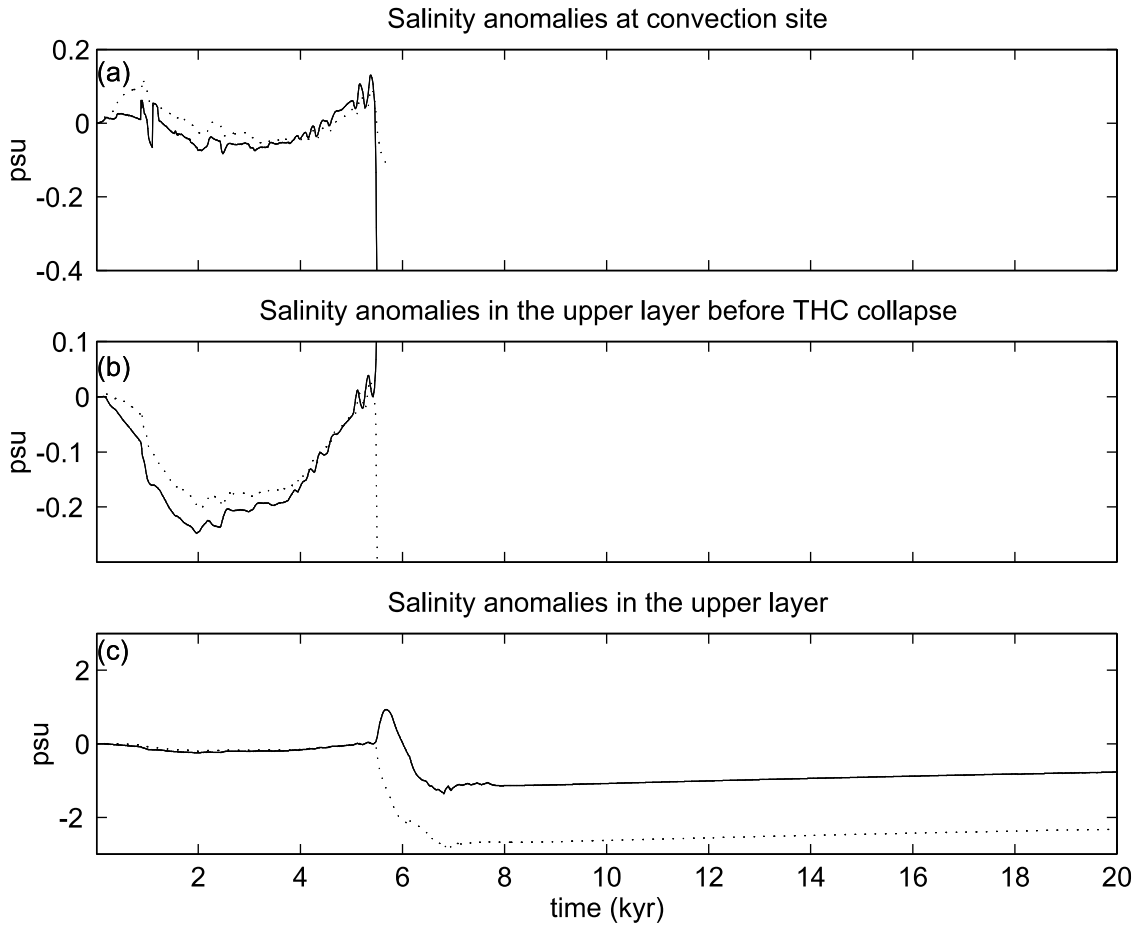

Figure 12. The time series of (a) the upper and lower layer salinity anomalies relative to their initial values at the convection site (around 62.5°N) (dotted line corresponds to lower layer; solid line corresponds to upper layer), (b) the low- and high-latitude salinity anomalies relative to their initial values in the upper layer before the THC collapse (dotted line corresponds to high latitudes; solid line corresponds to low latitudes), and (c) the low- and high-latitude salinity anomalies relative to their initial values in the upper layer for the whole model integration period (0–20 kyr) using a compressed vertical scale (dotted line corresponds to high latitudes; solid line corresponds to low latitudes) for the same experiment as in Figure 10.

in the upper layer for the same temperature anomaly. This is the reason that in Figure 10b the vertical density difference anomaly becomes negative first and then positive. Also, from Figure 11c, although the temperature anomaly drop in the high latitudes is larger than that in the low latitudes after 1 kyr, the difference between them becomes smaller after 4 kyr. Upon considering the nonlinear effect of the temperature change on the density, a smaller temperature anomaly causes a larger density change in the low latitudes (see Figure 10c), which may affect the meridional upper layer density gradient.

[41] Also, from the time series of the upper and lower layer salinity relative to their initial values at the convection site and the low- and high-latitude salinity relative to their initial values (Figure 12), salinity changes are found to be very small just before the THC collapses. (Note that in Figure 12b the low- and high-latitude salinities averaged over the upper layer decrease when the THC in the North Atlantic is intensified. This is due to the fact that an intensified THC enhances salt transport from the North Atlantic Ocean basin to the Antarctic Circumpolar Current (ACC) region. Further analysis (not shown) shows an increase of salinity in the ACC region as a consequence of the salinity decrease in the North Atlantic. This salinity anomaly then propagates to the Pacific Ocean on a millennial timescale. In the experiment with fixed oceanic freshwater flux we found similar results.) Simple calculations based on the equation of state used in the ocean model show that before the THC collapses the density changes due to the salinity changes only are one order of magnitude smaller than those due to the temperature changes only.

[42] Therefore we conclude that the climate-induced temperature changes alter the vertical stratification at the convection site and the meridional upper layer density gradient and hence are mainly responsible for the weakening and eventual collapse of the THC for a very cold climate.

5. Conclusions

[43] In this paper, a five-component (atmosphere, ocean, sea ice, land surface, and ice sheet) climate model of intermediate complexity (the so-called McGill Paleoclimate Model (MPM)) is employed to study the response of the global THC to various cold climates. These cold climates are realized by increasing the planetary emissivity in the MPM linearly over a 5-kyr period and then keeping it constant for another 15 kyr of model integration. The results presented are at the end of the model run (the last 5-kyr means). We recognize that each component in the MPM is rather simple compared with more comprehensive models, and

therefore there are many uncertainties in the model results. Although we cannot give precise details of the THC corresponding to various cold climates, the following results appear to be fairly robust: (1) A slightly cold climate may have a strong THC as compared to the present-day THC. A very cold climate may have a weaker or collapsed THC as compared to the present-day THC. (2) Model results suggest that the THC is relatively strong during the inception phase and early stage of a glaciation, while the THC is not strong (as compared to the present-day THC) or even weaker for a peak glacial. (3) The hydrological cycle might be responsible for a strong THC in a slightly cold climate. (4) The thermal factor is responsible for a weak or collapsed THC in a very cold climate. (5) The potential influence of surface temperature changes must be taken into account for a full understanding of the role of the THC in the climate system.

[44] **Acknowledgments.** We would like to thank A. Berger for kindly providing the code for calculating the solar insolation and T. Fichefet for providing the data used in their ocean model. We also thank Andrey Ganopolski and two anonymous reviewers for their constructive comments which helped to improve the paper. L. A. Mysak is indebted to the Canadian Natural Sciences and Engineering Research Council for sustained research support. J. F. McManus' contribution was made possible in part by the U.S. NSF and the Hoch Endowed Fund. He also thanks D. W. Oppo and J. L. Cullen for their support and generosity. This paper was revised while L.A.M. was visiting (winter 2001) the Institute for Climate Research, ETH Zürich, whose hospitality and support are gratefully acknowledged.

References

Berger, A. L., Long-term variations of daily insolation and Quaternary climatic changes, *J. Atmos. Sci.*, *35*, 2362–2367, 1978.

Boyle, E. A., and L. Keigwin, North Atlantic thermohaline circulation during the past 20,000 years linked to high-latitude surface temperature, *Nature*, *300*, 35–40, 1987.

Boyle, E. A., and P. Rosener, Further evidence for a link between Late Pleistocene North Atlantic surface temperatures and North Atlantic Deep-Water production, *Palaeogeogr. Palaeoclimatol. Palaeoecol.*, *89*, 113–124, 1990.

Broecker, W. S., and T.-H. Peng, *Tracers in the Sea*, Lamont-Doherty Earth Obs., Palisades, N. Y., 1982.

Chapman, M. R., and N. J. Shackleton, Millennial-scale fluctuations in North Atlantic heat flux during the last 150,000 years, *Earth Planet. Sci. Lett.*, *159*, 57–70, 1998.

Charles, C. D., and R. G. Fairbanks, Evidence from Southern Ocean sediments for the effect of North Atlantic deep-water flux on climate, *Nature*, *355*, 416–419, 1992.

Curry, W. B., and T. J. Crowley, The $\delta^{13}C$ of equatorial Atlantic surface waters: Implications for ice age pCO_2 levels, *Paleoceanography*, *2*, 489–517, 1987.

Dokken, T. M., and E. Jansen, Rapid changes in the mechanism of ocean convection during the last glacial period, *Nature*, *401*, 458–461, 1999.

Duplessy, J.-C., and N. J. Shackleton, Response of global deep-water circulation to Earth's climatic change 135,000-107,000 years ago, *Nature*, *316*, 500–507, 1985.

Duplessy, J.-C., N. J. Shackleton, R. G. Fairbanks, L. Labeyrie, D. Oppo, and N. Kallel, Deepwater source variations during the last climatic cycle and their impact on global deep-water circulation, *Paleoceanography*, *3*, 343–360, 1988.

Fanning, A. F., and A. J. Weaver, An atmospheric energy-moisture balance model: Climatology, interpentadal climate change, and coupling to an ocean general circulation model, *J. Geophys. Res.*, *101*, 15,111–15,128, 1996.

Flower, B. P., D. W. Oppo, J. F. McManus, K. A. Venz, D. A. Hodell, and J. Cullen, North Atlantic intermediate to deep water circulation and chemical stratification during the past 1 m.y., *Paleoceanography*, *15*, 388–403, 2000.

Fronval, T., and E. Jansen, Eemian and early Weichselian (140–60 ka) paleoceanography and paleoclimate in the Nordic Seas with comparisons to Holocene conditions, *Paleoceanography*, *12*, 443–462, 1997.

Gallée, H., J. P. van Ypersele, T. Fichefet, I. Marsiat, C. Tricot, and A. L. Berger, Simulation of the last glacial cycle by a coupled sectorially averaged climate-ice sheet model, 2, Response to insolation and CO_2 variations, *J. Geophys. Res.*, *97*, 15,713–15,740, 1992.

Ganopolski, A., S. Rahmstorf, V. Petoukhov, and M. Claussen, Simulation of modern and glacial climates with a coupled global model of intermediate complexity, *Nature*, *391*, 351–356, 1998.

Gordon, H. B., and S. P. O'Farrell, Transient climate change in the CSIRO coupled model with dynamic sea ice, *Mon. Weather Rev.*, *125*, 875–907, 1997.

Harvey, L. D. D., Development of a sea ice model for use in zonally averaged energy balance climate models, *J. Clim.*, *1*, 1221–1238, 1988.

Hays, J. D., J. Imbrie, and N. J. Shackleton, Variations in the Earth's orbit: Pacemaker of the Ice Ages, *Science*, *194*, 1121–1132, 1976.

Hellerman, S., and M. Rosenstein, Normal monthly wind stress over the world ocean with error estimates, *J. Phys. Oceanogr.*, *13*, 1093–1104, 1983.

Hibler, W. D. III, A dynamic thermodynamic sea ice model, *J. Phys. Oceanogr.*, *9*, 815–846, 1979.

Houghton, J. T., L. G. Meira Filho, D. J. Griggs, and K. Maskell, An introduction to simple climate models used in the IPCC second assessment report, *IPCC Tech. Pap. II*, 47 pp., Intergov. Panel on Clim. Change, Geneva, Switzerland, 1997.

Hughes, T. M. C., and A. J. Weaver, Multiple equilibria of an asymmetric two-basin ocean model, *J. Phys. Oceanogr.*, *24*, 619–637, 1994.

Imbrie, J., J. D. Hays, D. G. McIntyre, A. C. Mix, J. J. Morley, N. G. Pisias, W. L. Prell, and N. J. Shackleton, The orbital theory of Pleistocene climate: Support from a revised chronology of the marine $\delta^{18}O$ record, in *Milankovitch and Climate*, edited by A. Berger et al., pp. 269–305, D. Reidel, Norwell, Mass., 1984.

Johnson, R. G., and J. T. Andrews, Rapid ice sheet growth and initiation of the last glaciation, *Quat. Res.*, *12*, 119–134, 1979.

Keigwin, L. D., and E. A. Boyle, Carbon isotopes in deep-sea benthic foraminifera: Precession and changes in low-latitude biomass, in *The Carbon Cycle and Atmospheric CO_2: Natural variations Archean to Present*, *Geophysical Monogr. Ser.*, vol. 32, pp. 319–328, AGU, Washington, D. C., 1985.

Kroopnick, P., The distribution of ^{13}C in the Atlantic Ocean, *Earth Planet. Sci. Lett.*, *49*, 469–484, 1980.

Labeyrie, L., J.-C. Duplessy, and P. L. Blanc, Variations in the mode of formation and temperature of oceanic deep waters over the past 125,000 years, *Nature*, *327*, 477–482, 1987.

Labeyrie, L., H. Leclaire, C. Waelbroeck, E. Cortijo, J.-C. Duplessy, L. Vidal, M. Elliot, B. Le Coat, and G. Auffret, Temporal variabiliity of the surface and deep waters of the north west Atlantic Ocean at orbital and millennial scales, in *Mechanisms of Global Climate Change at Millennial Time Scales*, *Geophys. Monogr. Ser.*, vol. 112, edited by P. U. Clark, R. S. Webb, and L. D. Keigwin, pp. 77–98, AGU, Washington, D. C., 1999.

Ledley, T. S., The climatic response to meridional sea-ice transport, *J. Clim.*, *4*, 147–163, 1991.

Levitus, S., *Climatological Atlas of the World Ocean*, *NOAA Prof. Pap. 13*, Natl. Oceanic and Atmos. Admin., Silver Spring, Md., 1982.

Lohmann, G., and R. Gerdes, Sea ice effects on the sensitivity of the thermohaline circulation, *J. Clim.*, *11*, 2789–2803, 1998.

Lynch-Steiglitz, J., and R. G. Fairbanks, A conservative tracer for glacial ocean circulation from carbon isotope and paleo-nutrient measurements in benthic foraminifera, *Nature*, *369*, 41–43, 1994.

Lynch-Steiglitz, J., W. B. Curry, and N. Slowey, Weaker Gulf Stream in the Florida Straits during the Last Glacial Maximum, *Nature*, *402*, 644–648, 1999.

Mackensen, A., H. W. Hubberten, T. Bickert, G. Fischer, and D. K. Fütterer, $\delta^{13}C$ in benthic foraminiferal tests of *Fontabia wuellerstorfi* (Schwager) relative to $\delta^{13}C$ of dissolved inorganic carbon in Southern Ocean deep water: Implications for glacial ocean circulation models, *Paleoceanography*, *8*, 587–610, 1993.

Manabe, S., Climate and the ocean circulation, I, The atmospheric circulation and the hydrology of the Earth surface, *Mon. Weather Rev.*, *97*, 739–774, 1969.

Manabe, S., and R. J. Stouffer, Two stable equilibria of a coupled ocean-atmosphere model, *J. Clim.*, *1*, 841–866, 1988.

Manabe, S., and R. J. Stouffer, Multiple-century response of a coupled ocean-atmosphere model to an increase of atmospheric carbon dioxide, *J. Clim.*, *7*, 5–23, 1994.

Manabe, S., R. J. Stouffer, M. J. Spelman, and K. Bryan, Transient responses of a coupled ocean-atmosphere model to a gradual changes of atmospheric CO_2, part I, Annual mean response, *J. Clim.*, *4*, 785–818, 1991.

Marotzke, J., and J. Willebrand, Multiple equilibria of the global thermohaline circulation, *J. Phys. Oceanogr.*, *21*, 1372–1385, 1991.

McManus, J. F., D. W. Oppo, D. A. Hodell, J. L. Cullen, M. Stievenard, and J. Jouzel, Comparison of long climate records from cores recovered by deep drilling on Antarctica and in the North Atlantic, *Eos Trans. AGU*, *79*(45), Fall Meet. Suppl., F149, 1998.

McManus, J. F., D. W. Oppo, and J. L. Cullen, A 0.5-million-year record of millennial-scale climate variability in the North Atlantic, *Science*, *283*, 971–975, 1999.

McManus, J. F., D. W. Oppo, L. D. Keigwin, J. L. Cullen, and G. C. Bond, Thermohaline circulation and prolonged interglacial warmth in the North Atlantic, *Quat. Res.*, in press, 2002.

Milankovitch, M. M., Mathematische Klimalehre und astronomische Theorie der Klimaschwankungen, in *Handbuch der Klimatologie*, edited by W. Koppen and R. Geiger, Gebrüder Borntraeger, Stuttgart, Germany, 1930.

Milankovitch, M. M., *Canon of insolation and the ice-age problem*, Koniglich Serbische Akad., Belgrade, Yugoslavia, 1941.

Mix, A. C., and R. G. Fairbanks, North Atlantic surface-ocean control of Pleistocene deep-ocean circulation, *Earth Planet. Sci. Lett.*, *73*, 231–243, 1985.

Mix, A. C., N. G. Pisias, W. Rugh, J. Wilson, A. Morey, and T. K. Hagelberg, Benthic foraminifer stable isotope record from Site 849 (0-5 MA): Local and global climate changes, *Proc. Ocean Drill. Program Sci. Results*, *138*, 371–391, 1995.

Mysak, L. A., and Z. Wang, The McGill Paleoclimate Model (MPM): A new Earth system model of intermediate complexity, *Can. Meteorol. Oceanogr. Soc. Bull.*, *28*, 104–109, 2000.

Ninnemann, U. S., C. D. Charles, and D. A. Hodel, Origin of global millennial scale climate events: Constraints from the Southern Ocean, in *Mechanisms of Global Climate Change on Millennial Time Scales*, *Geophys. Monogr. Ser.*, vol. 112, edited by P. U. Clark, R. S. Webb, and L. D. Keigwin, pp. 99–112, AGU, Washington, D. C., 1999.

Oerlemans, J., Some basic experiments with a vertically integrated ice sheet model, *Tellus*, *33*, 1–11, 1981.

Oppo, D. W., and R. G. Fairbanks, Variability in the deep and intermediate water circulation of the Atlantic Ocean during the past 25,000 years: Northern Hemisphere modulation of the Southern Ocean, *Earth Planet. Sci. Lett.*, *86*, 1–15, 1987.

Oppo, D. W., and S. J. Lehman, Mid-depth circulation of the subpolar North Atlantic during the Last Glacial Maximum, *Science*, *259*, 1148–1152, 1993.

Oppo, D. W., and S. J. Lehman, Suborbital timescale variability of North Atlantic Deep Water during the past 200,000 years, *Paleoceanography*, *10*, 901–910, 1995.

Oppo, D. W., M. Horowitz, and S. J. Lehman, Marine core evidence for reduced deep water production during Termination 2 followed by a relatively stable substage 5e, *Paleoceanography*, *12*, 51–63, 1997.

Oppo, D. W., J. F. McManus, and J. L. Cullen, Abrupt climate events 500,000 to 340,000 years ago: Evidence from subpolar North Atlantic sediments, *Science*, *279*, 1335–1338, 1998.

Peltier, W. R., and S. Marshall, Coupled energy-balance/ice-sheet model simulations of the glacial cycle: A possible connection between terminations and terrigenous dust, *J. Geophys. Res.*, *100*, 14,269–14,289, 1995.

Prange, M., G. Lohmann, and R. Gerdes, Sensitivity of the thermohaline circulation for different climates—Investigations with a simple atmosphere-ocean model, *Paleoclimates*, *2*, 71–99, 1997.

Rahmstorf, S., On the fresh water forcing and transport of the Atlantic thermohaline circulation, *Clim. Dyn.*, *12*, 799–811, 1996.

Rahmstorf, S., and A. Ganopolski, Long-term global warming scenarios computed with an efficient coupled climate model, *Clim. Change*, *43*, 353–367, 1999.

Raymo, M. E., The timing of major climate terminations, *Paleoceanography*, *12*, 577–585, 1997.

Raymo, M. E., W. F. Ruddiman, N. J. Shackleton, and D. W. Oppo, Evolution of Atlantic-Pacific $\delta^{13}C$ gradients over the last 2.5 m. y., *Earth Planet. Sci. Lett.*, *97*, 353–368, 1990.

Rohling, E. J., M. Fenton, F. J. Jorissen, P. Bertrand, G. Ganssen, and J. P. Coulet, Magnitudes of sea level lowstands of the past 500,000 years, *Nature*, *394*, 162–165, 1998.

Ruddiman, W. F., A. McIntyre, V. Niebler-Hunt, and J. T. Durazzi, Ocean evidence for the mechanism of rapid Northern Hemisphere glaciation, *Quat. Res.*, *13*, 33–64, 1980.

Sarnthein, M., and R. Tiedemann, Toward a high-resolution stable isotope stratigraphy of the last 3.4 million years: Sites 658 and 659 off Northwest Africa, *Proc. Ocean Drill. Program Sci. Results*, *108*, 167–185, 1989.

Sarnthein, M., et al., Changes in east Atlantic deepwater circulation over the last 30,000 years: Eight time slice reconstructions, *Paleoceanography*, *9*, 209–267, 1994.

Schmidt, G. A., and L. A. Mysak, The stability of a zonally averaged thermohaline circulation model, *Tellus, Ser. A*, *48*, 158–178, 1996.

Seidov, D., M. Sarnthein, K. Stattegger, R. Prien, and M. Weinelt, North Atlantic Ocean circulation during the Last Glacial Maximum and subsequent meltwater event: A numerical model, *J. Geophys. Res.*, *101*, 16,305–16,332, 1996.

Semtner, A. J., A model for the thermodynamic growth of sea ice in numerical investigations of the climate, *J. Phys. Oceanogr.*, *6*, 379–389, 1976.

Shackleton, N. J., Carbon-13 in Uvigerina: Tropical rain forest history and the equatorial Pacific carbonate dissolution cycles, in *The Fate of Fossil Fuel CO_2 in the Oceans*, edited by N. R. Andersen and A. Malahoff, pp. 401–427, Plenum, New York, 1977.

Shackleton, N. J., Oxygen isotopes, ice volume and sea level, *Quat. Sci. Rev.*, *6*, 183–190, 1987.

Shackleton, N. J., and N. G. Pisias, Atmospheric carbon dioxide, orbital forcing, and climate, in *The Carbon Cycle and Atmospheric CO_2: Natural Variations Archean to Present*, *Geophys. Monogr. Ser.*, vol. 32, pp. 303–317, AGU, Washington, D. C., 1985.

Shackleton, N. J., M. A. Hall, J. Line, and C. Shuxi, Carbon isotope data in core V19-30 confirm reduced carbon dioxide concentration in the ice age atmosphere, *Nature*, *306*, 319–322, 1983.

Shackleton, N. J., J.-C. Duplessy, M. Arnold, P. Maurice, M. A. Hall, and J. Cartlidge, Radiocarbon age of last glacial Pacific deep water, *Nature*, *335*, 708–711, 1988.

Spero, H. J., J. Bijma, D. W. Lea, and B. E. Bemis, Effects of seawater carbonate concentration on foraminiferal carbon and oxygen isotopes, *Nature*, *390*, 497–500, 1997.

Stocker, T. F., Past and future reorganisations in the climate system, *Quat. Sci. Rev.*, *19*, 301–319, 2000.

Stocker, T. F., and A. Schmittner, Influence of CO_2 emission rate on the stability of the thermohaline circulation, *Nature*, *388*, 862–864, 1997.

Stocker, T. F., D. G. Wright, and L. A. Mysak, A zonally averaged, coupled ocean-atmosphere model for paleoclimate studies, *J. Clim.*, *5*, 773–797, 1992.

van Kreveld, S. A., M. Sarnthein, H. Erlenkeuser, P. Grootes, S. Jung, M. J. Nadeau, U. Pflaumann, and A. Voelker, Potential links between surging ice sheets, circulation changes and the Dansgaard-Oeschger cycles in the Irminger Sea, 60-18 kyr, *Paleoceanography*, *15*, 425–442, 2000.

Vidal, L., L. Labeyrie, E. Cortijo, M. Arnold, J.-C. Duplessy, E. Michel, S. Becque, and T. C. E. van Weering, Evidence for changes in the North Atlantic Deep Water linked to meltwater surges during the Heinrich events, *Earth Planet. Sci. Lett.*, *146*, 13–27, 1997.

Wang, Z., and L. A. Mysak, A simple coupled atmosphere-ocean-sea ice-land surface model for climate and paleoclimate studies, *J. Clim.*, *13*, 1150–1172, 2000.

Wang, Z., and L. A. Mysak, Ice sheet-thermohaline circulation interactions in a climate model of intermediate complexity, *J. Oceanogr.*, *57*, 481–494, 2001.

Weaver, A. J., M. Eby, A. F. Fanning, and E. C. Wiebe, Simulated influence of carbon dioxide, orbital forcing and ice sheets on the climate of the Last Glacial Maximum, *Nature*, *394*, 847–853, 1998.

Winton, M., The effect of cold climate upon North Atlantic Deep Water formation in a simple ocean-atmosphere model, *J. Clim.*, *10*, 37–51, 1997.

Wright, D. G., An equation of state for use in ocean models: Eckart's formula revisited, *J. Atmos. Oceanic Technol.*, *14*, 735–740, 1997.

Wright, D. G., and T. F. Stocker, A zonally averaged ocean model for the thermohaline circulation, I, Model development and flow dynamics, *J. Phys. Oceanogr.*, *21*, 1713–1724, 1991.

Yu, E.-F., R. Francois, and M. P. Bacon, Similar rates of modern and last-glacial ocean thermohaline circulation inferred from radiochemical data, *Nature*, *379*, 689–694, 1996.

L. A. Mysak and Z. Wang, Department of Atmospheric and Oceanic Sciences, McGill University, Montreal, Quebec H3A 2K6, Canada. (wangz@zephyr.meteo.mcgill.ca)

J. F. McManus, Department of Geology and Geophysics, Woods Hole Oceanographic Institution, Woods Hole, MA 02543, USA.